Available online at www.sciencedirect.com
SCIENCE DIRECT®
Journal of the European Ceramic Society 26 (2006) 1221–1229
www.elsevier.com/locate/jeurceramsoc

How Cr_2O_3 influences the microstructure and nonohmic features of the $SnO_2(Co_x, Mn_{1-x})O$-based varistor system

W.K. Bacelar [a], P.R. Bueno [b,*], E.R. Leite [a], E. Longo [a], J.A. Varela [b]

[a] *Interdisciplinary Laboratory of Electrochemistry and Ceramics, Department of Chemistry, Federal University of São Carlos, C. Postal 676, 13565-905 São Carlos, SP, Brazil*
[b] *Instituto de Química, Universidade Estadual Paulista, P.O. Box 355, 14801-907 Araraquara, SP, Brazil*

Received 10 July 2004; received in revised form 20 December 2004; accepted 16 January 2005
Available online 16 March 2005

Abstract

An investigation was made to discover how the addition of Cr_2O_3 affects the microstructural heterogeneity and nonohmic features of the $SnO_2(Co_x, Mn_{1-x})O$-based varistor system, with x varying from 0 to 1. The presence of Cr_2O_3 was found to strongly increase the nonohmic features when $x = 1$. However, the nonohmic features of the system decrease when x drops from 1 to 0, a behavior explained by the increase of the junction heterogeneity within the system's microstructure, accompanied by an excess of precipitates at the triple point in the grain boundary region due to modified MnO sintering. The presence of these precipitates causes the leakage current to increase in response to the creation of an ineffective barrier. The effect produced by heat-treating these systems in oxygen- and nitrogen-rich atmospheres suggests that, according to mechanisms previously discussed in the literature, Cr_2O_3 is more susceptible to oxygen, so that increasing the amount of oxygen in the grain boundary region may improve the system's nonohmic properties.

Keyword: Varistor; Cr_2O_3; SnO_2; Microstructure-final

1. Introduction

A varistor device is a nonlinear resistor displaying a nonohmic current–voltage behavior, which can be used as an over-voltage protector device.[1–3] The nonlinear features of current and voltage derive from the existence of potential barriers between the grain boundaries of the ceramic polycrystalline microstructure of varistor devices.[1] These potential barriers are usually of the Schottky-type in ZnO-based varistors,[2] which are the most commonly employed commercial varistor systems.[2] However, other polycrystalline systems have also been emerging for potential application as commercial devices, as in the case of SnO_2 and TiO_2 ceramic matrix-based devices.[4–9]

The nonohmic properties of SnO_2 n-type semiconductors with tetragonal crystalline structures are equivalent to those of the commercial ZnO varistor, although they present better thermal conductivity, which is an important anti-degradation factor. The SnO_2 bandgap is about 3.6 eV, although, in practice, the existing intrinsic oxygen vacancies form shallow donor levels with energies between 0.03 and 0.15 eV below the conduction band.[10,11] From the standpoint of the features of polycrystalline SnO_2, because this material presents low densification after sintering, it is used mostly in gas sensor applications.[12–15] To render it useful in other applications requiring higher densification levels, the addition of specific dopants, such as CoO to SnO_2 polycrystalline ceramics leads to high densification, thus, making it possible to obtain nonohmic features.[6] In fact, the SnO_2-based varistor can be obtained by adding densifying dopants, such as CoO, MnO and ZnO[16] in amounts exceeding 0.5 mol%.[17–21] It is believed that such oxide dopants facilitate mass transport throughout the grain boundary region, increasing densification of the polycrystalline matrix.[18,19] It should be noted that the most widely stud-

* Corresponding author.
E-mail address: prbueno@iq.unesp.br (P.R. Bueno).

0955-2219/$ – see front matter © 2005 Elsevier Ltd. All rights reserved.
doi:10.1016/j.jeurceramsoc.2005.01.051

ied densifying dopant used in SnO_2-based varistor systems is CoO.[22–26]

Once SnO_2 polycrystalline ceramics have densified, their nonohmic features can be obtained by adding Nb_2O_5, which favors the grain's electrical conductivity. Other dopants, such as chromium oxide (Cr_2O_3) can improve the nonohmic features by influencing the formation and characteristics of the potential barrier at the grain boundary.[6–9] Accordingly, the latter dopants can influence the nonohmic features in different ways and, therefore, the values of the nonlinear coefficient (α), which is an indicator of varistor efficiency.

The potential barrier in polycrystalline ceramics displays a behavior similar to barrier-injection transit-time diodes,[23–26] with the grain possessing an n-type feature and the grain-boundary a p-type feature. The presence of excess oxygen at grain boundaries in relation to the grain produces a p-type semiconductor feature (a metal-deficient and oxygen-rich phase), because of p-type semiconductor dopant segregated as metal atoms or precipitating as a new phase[23–26]. Therefore, the value of the nonlinear coefficient in SnO_2-based varistors can be optimized by an appropriate doping level of either a donor (Nb^{5+}) and/or an acceptor type (Cr^{3+}, Co^{2+}, Mn^{2+}/Mn^{3+}).[6–9,23–27]

The features of the electrical potential barrier, therefore, result from the chemical potential equilibrium between the grain and the grain boundary region during the sintering stage. In other words, the electrical potential barrier is formed by atomic-associated electronic defects at grain boundary interfaces, which are compensated in the depletion layer by positive entities, such as $V_O^{\cdot\cdot}$, $M_{Sn}^{\cdot}$. The main defects in the interfacial region which are compensated by positive charges of the depletion layer are $V_{Sn}^{////}$, O_{ads}', O_{ads}'', $O_{2(ads)}'$.[23–26,28] Accordingly, the height of potential barriers can be modulated by the amount of oxygen present at the grain-grain junction interface in SnO_2-based varistors. In a SnO_2-based varistor system doped with Cr_2O_3, the excess oxygen at the grain boundary can be controlled by the presence of segregated chromium metal atoms or Cr_2O_3 homogeneously precipitated as a new phase.[23–26,28] The degradation of the potential barriers of SnO_2-based varistors when these devices are subjected to heat treatment in nitrogen-rich atmospheres, and the subsequent restoration of the potential barriers to their original values after the material is subjected to a reheating treatment in an oxygen-rich atmosphere, reinforces the assumption that the balance of oxygen between grain and grain boundary to some extent controls the nonohmic properties.[24,28]

A detailed evaluation of the microstructural features of different dense SnO_2·MnO polycrystalline ceramic compositions was made recently by means of an analytical electron microscope (AEM) equipped with an X-ray energy dispersive spectrometer (XEDS). As foreseen, the microstructural features proved to exert a very important effect on the nonohmic properties. However, the main features of the microstructure controlling the nonohmic behavior were detected with the aid of admittance/dielectric spectroscopy.[29,30] Although the addition of both CoO and MnO leads to high densification of SnO_2 polycrystalline ceramics, it was found that MnO applied as a densifying agent of the SnO_2 matrix (rather than CoO) produces different nonohmic features due to its dissimilar sintering mechanism and densification rate, with consequences on the nonohmic electrical properties. Moreover, the authors demonstrated that SnO_2·CoO-based ceramics are more homogeneous than SnO_2·MnO-based ceramics,[29,30] which contain a precipitate phase (Mn_2SnO_4), mainly at triple points of the grain boundary. Excessive amounts of precipitate phases at triple points of the grain boundary generally cause the leakage current to increase and the nonlinear coefficient value to decrease, as discussed in ref.[31]

In this study, we examined the influence of the Cr_2O_3 concentration on $SnO_2(Co_xMn_{1-x})O$-based systems doped with a fixed amount of 0.05 mol% of Nb_2O_5, in order to discover how excessive amounts of this dopant influence the microstructural features and, hence, the nonohmic properties of $SnO_2(Co_xMn_{1-x})O$-based varistors. The degrading effect of MnO on the nonohmic features was also confirmed by its replacement with CoO, despite the high densification achieved, reinforcing the evidence reported in refs.[29,30]

2. Experimental procedure

The powders were processed using the conventional methods for mixing oxides in alcoholic media. The oxides employed, all of analytical grade, were: SnO_2 (CESBRA), Nb_2O_5 (CBMM), Cr_2O_3 (Merck), CoO (Riedel) and MnO_2 (Riedel). The compositions studied in the present work were prepared using molar percentages. The powders were uniaxially pressed into a cylindrical shape (11.0 mm × 1.3 mm) and then isostatically pressed at 150 MPa. The samples were sintered in an ambient atmosphere at 1300 °C for 1.5 h, at a heating rate of 10 °C min^{-1} and a cooling rate of 2 °C min^{-1}. The relative densities of the samples (green and sintered) were identified using a mercury porosimeter (Micromeritics 9320). The samples were polished and silver electrodes were placed on the ceramic surfaces before their electrical characterization, which was performed by means of *I–V* measurements with a Keithley 237 current source. The samples' leakage current was measured in a direct current system in a fixed electric field corresponding to 85% of $E_{0.05}$, where $E_{0.05}$ is the electric field corresponding to a current density of 0.05 mA cm^{-2}. This electric field was chosen because its value corresponds to the region where the electric conductivity is mostly controlled by grain boundaries.[3]

X-ray diffraction (SIEMENS D-5000) was used to structurally characterize the ceramic phases. Scanning electron microscopy (DSM 940-A) was used to analyze the samples' microstructures. The mean grain size was determined by SEM micrographs, using the PGT software (ASTM-E112) program. The material's surface was mapped by energy dispersive spectroscopy (EDS).

The molar concentrations of SnO_2-based varistor systems studied here were based on the two formulae: 98.975

Table 1
Experimental (d_{ex}) and relative densities (d_{rt}) and mean grain size values obtained at 1300 °C for 1.5 h as a function of molar percentage of dopants

System	Cr_2O_3 (mol%)	MnO_2 (mol%)	CoO (mol%)	d_{ex} (g cm^{-3})	d_{rt} (%)	$\bar{d}$ (μm)
S1	0.000	0.000	1.000	6.88	98.99	5.03
S2	0.000	0.250	0.750	6.84	98.32	6.90
S3	0.000	0.500	0.500	6.74	97.00	4.82
S4	0.025	0.000	1.000	6.40	92.05	5.01
S5	0.025	0.250	0.750	6.35	91.36	5.83
S6	0.025	0.500	0.500	6.20	89.21	6.69
S7	0.025	0.750	0.250	5.70	81.97	7.48
S8	0.025	1.000	0.000	5.67	81.58	8.35

The experimental and relative densities were calculated from the crystal's theoretical density.

SnO_2–1.000 (Co_x, Mn_{1-x})O–0.025 Nb_2O_5 and 98.950 SnO_2–1.000 (Co_x, Mn_{1-x})O–0.025 Nb_2O_5–0.025 Cr_2O_3. Each system with different values of x was named Sj, where $j = 1, 2, \ldots, 8$. Thus, in S1, $x = 0.000$; in S2, $x = 0.250$; in S3, $x = 0.500$ and so on. The formulae of systems containing Cr_2O_3 were 98.950 SnO_2–1.000 (Co_{1-x}, Mn_x)O–0.025 Nb_2O_5–0.025 Cr_2O_3. Thus, in S4, $x = 0.000$; in S5, $x = 0.250$; in S6, $x = 0.500$; in S7, $x = 0.750$; and in S8, $s = 1.000$. To facilitate the visualization of the systems' compositions, Table 1 summarizes all the compositions studied. These compositions were thermally treated at 900 °C for 1 h in O_2-rich and N_2-rich atmospheres, similarly to the treatments reported in refs.[24,28] It is important to mention that the addition of MnO_2 is equivalent to adding MnO, because Mn^{2+} is the valence most likely to remain stable in SnO_2 after sintering.[32]

3. Results and discussion

3.1. Microstructural characteristics as a function of Cr_2O_3 and MnO concentrations

According to what was discussed in the introduction, the choice of the appropriate dopants may influence a varistor system's n–p–n characteristics. The bulk region inside the grain may present an n-type semiconductor feature with a high concentration of oxygen vacancies and a donor-type dopant, while the grain boundary region displays a p-type feature (because the bulk's matrix-metal environment is an oxygen-deficient region in comparison with the grain boundary region, which is rich in oxygen due to segregated transition metal).

In the case of SnO_2-based varistors, the substitution of Sn^{4+} in the matrix lattice for acceptor atoms, such as Co^{2+}, Co^{3+}, Mn^{2+}, Mn^{3+}, Cr^{2+} and Cr^{3+} can lead to the formation of acceptor states in the forbidden band gap of SnO_2, which can be compensated by oxygen vacancies. Such oxygen vacancies may be one of the defects responsible for the sintering of the system.[18,19] The main solid-state reactions are represented below:

$$MnO \xrightarrow{SnO_2} Mn''_{sn} + V^{\cdot\cdot}_O + O^x_O, \quad (1)$$

$$CoO \xrightarrow{SnO_2} Co''_{sn} + V^{\cdot\cdot}_O + O^x_O, \quad (2)$$

$$Cr_2O_3 \xrightarrow{SnO_2} 2Cr'_{sn} + V^{\cdot\cdot}_O + 3O^x_O. \quad (3)$$

Thus, it is likely that the oxygen vacancies are conducted into the grain's bulk, while the Mn''_{sn}, Mn'_{sn}, Co''_{sn} and Cr'_{sn} species migrate to the grain boundary region. The presence of segregated metals in the grain boundary region causes that region to become enriched with oxygen species, because such metals form a p-type region in which the ceramic matrix bulk is oxygen-deficient compared with the grain boundary, so that an excess of oxygen species is possible at the grain-grain interface.

The electronic conductivity in the lattice of SnO_2 polycrystalline ceramic grains can be increased by the addition of Nb_2O_5, according to the following equation:

$$2Nb_2O_5 \xrightarrow{SnO_2} 4Nb^{\cdot}_{sn} + V^{''''}_{sn} + 10O^x_O, \quad (4)$$

The ions in Nb ion-doped SnO_2 act as shallow donors that provide the conduction band with an electronic state, according to the reaction:

$$Nb^x_{Sn} \rightarrow Nb^{\cdot}_{sn} + e'. \quad (5)$$

Mn''_{sn}, Mn'_{sn}, Co''_{sn} and Cr'_{sn} species were formed in the grain boundary, according to Eqs. (1)–(3), likely trapping the free electrons released by $Nb^{\cdot}_{sn}$, according to Eq. (5), and thereby creating a potential barrier in the grain boundary region. The height and width of this potential barrier was dependent on the degree of oxidation of the grain boundary relative to that of the bulk.

As already known and reported by other authors, the X-ray diffraction pattern of SnO_2-based varistor does not present any other phase apart from cassiterite with a single rutile-type structure.[6–9] However, in the present case, since the concentration of MnO dopants was increased, the presence of precipitate phases was visible by SEM (the micrographs in Figs. 1 and 2 illustrate this fact, but ref.[29] discusses this phenomenon in detail). To analyze these precipitated phases, which are below X-ray accuracy, an analysis by scanning electron microscopy coupled with energy dispersive spectroscopy was performed. Fig. 2 illustrates the microstructure obtained for the S5 composition. More detailed discussions of the microstructural features of SnO_2 fully based on MnO as the main sintering dopant, i.e., without CoO, are given elsewhere.[29,30] The microstructures observed here were di-

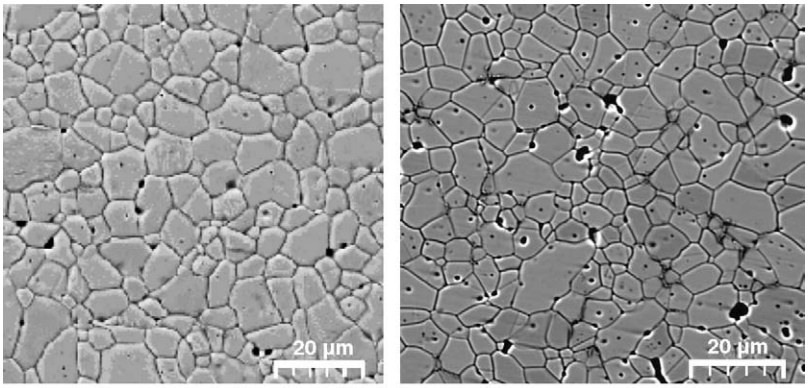

Fig. 1. Micrographs of the (a) S2 and (b) S8 compositions; both sintered at 1300 °C for 1.5 h.

versified, changing according to the concentration of dopant, and displaying pores and a precipitate phase at the triple point of the grain boundaries.[29,30]

The effect of MnO on the sintering of SnO_2 was analyzed by Paria et al.,[33] who proposed a mass transport mechanism based on viscous flow to explain the densification promoted by MnO dopant. Castro and Aldao, Cerri et al. and Varela et al.[16,18,19] also observed high densification of SnO_2 with the addition of MnO at concentrations exceeding 0.5 mol% (relative density above 95%) in a similar system. These authors ascribed the effect of MnO to the formation of oxygen vacancies in the SnO_2 lattice, which could promote mass transport in the lattice. The formation of Mn_2SnO_4 and $MnSnO_3$ in the grain boundary region has also been reported.[18,19] Therefore, modifying the SnO_2 crystal by adding CoO or MnO may alter the sintering mechanisms and densification rate. Hence, doping SnO_2 with MnO or CoO leads to the creation of additional oxygen vacancies, which in turn increase the diffusion rate of oxygen ions and alter the sintering of SnO_2 polycrystals. However, SnO_2·CoO-based ceramics have a more homogeneous microstructure than do SnO_2·MnO-based ceramics, a fact clearly visible from the presence of precipitate phase in the latter, mainly at triple points of the grain boundary. Therefore, the solubility of Mn^{2+} atoms in the SnO_2 matrix appears to be lower than that of Co^{2+} in the SnO_2 matrix.

As pointed out in ref.,[31] when precipitates are present in higher concentrations at triple points, they can affect the nature of SnO_2–SnO_2 junctions and, hence, the number of active barriers. Once the precipitates are present in triple junctions of the microstructure, they can cause adjacent SnO_2–SnO_2 junctions poor in segregated metal atoms because precipitates consume the segregated metal atoms in regions adjacent to them. Such adjacent regions generate junctions that may present non-effective potential barriers, so that a parallel conduction through these non-active barriers may occur in varistor devices. This parallel conduction is responsible for an increase of leakage current. Sometimes, heat treatments in oxygen-rich atmospheres cannot increase the potential barrier and density of states at the interface, because the oxygen species may be consumed preferentially, eliminating the non-active potential barrier in regions with lower concentrations of segregated metal and enriching the precipitates with oxygen species.

Our analysis of SEM micrographs indicates that the addition of MnO causes an increase of precipitate phase at triple points of the grain boundary, accompanied by an increase of the leakage current (and a decrease of α values, see Tables 2 and 3 and refs.[29,30]), which is in agreement with the proposal of Simões et al.[31] and is summarized above.

If the mass transport is fast during the sintering process, it can give rise to the formation of extra grain pores.[34,35] Therefore, the substitution of CoO atoms for MnO can probably change the mass transport mechanism during the sintering process, inducing the formation of a greater concentration of

Table 2
Nonlinearity coefficient (α), breakdown electric field (E_r) and potential barrier per grain (ν_b) for the S*j* composition in different atmospheres

System	α				E_r (V cm^{-1})				ν_b (V per barrier)	
	Air	O_2	N_2	re-O_2	Air	O_2	N_2	re-O_2	Air	re-O_2
S1	21	23	12	24	4920	5127	2815	5206	2.86	3.03
S2	11	12	10	13	2888	2927	2810	3083	1.99	2.12
S3	12	13	12	14	3612	3695	3574	3710	1.74	1.88
S4	49	65	46	75	4106	4382	4136	4575	2.06	2.30
S5	21	28	19	35	4000	5108	3980	5925	2.33	3.45
S6	14	18	13	27	5904	6814	6636	6947	3.95	4.64
S7	13	–	–	–	16848	–	–	–	12.6	–
S8	–	–	–	–	–	–	–	–	–	–

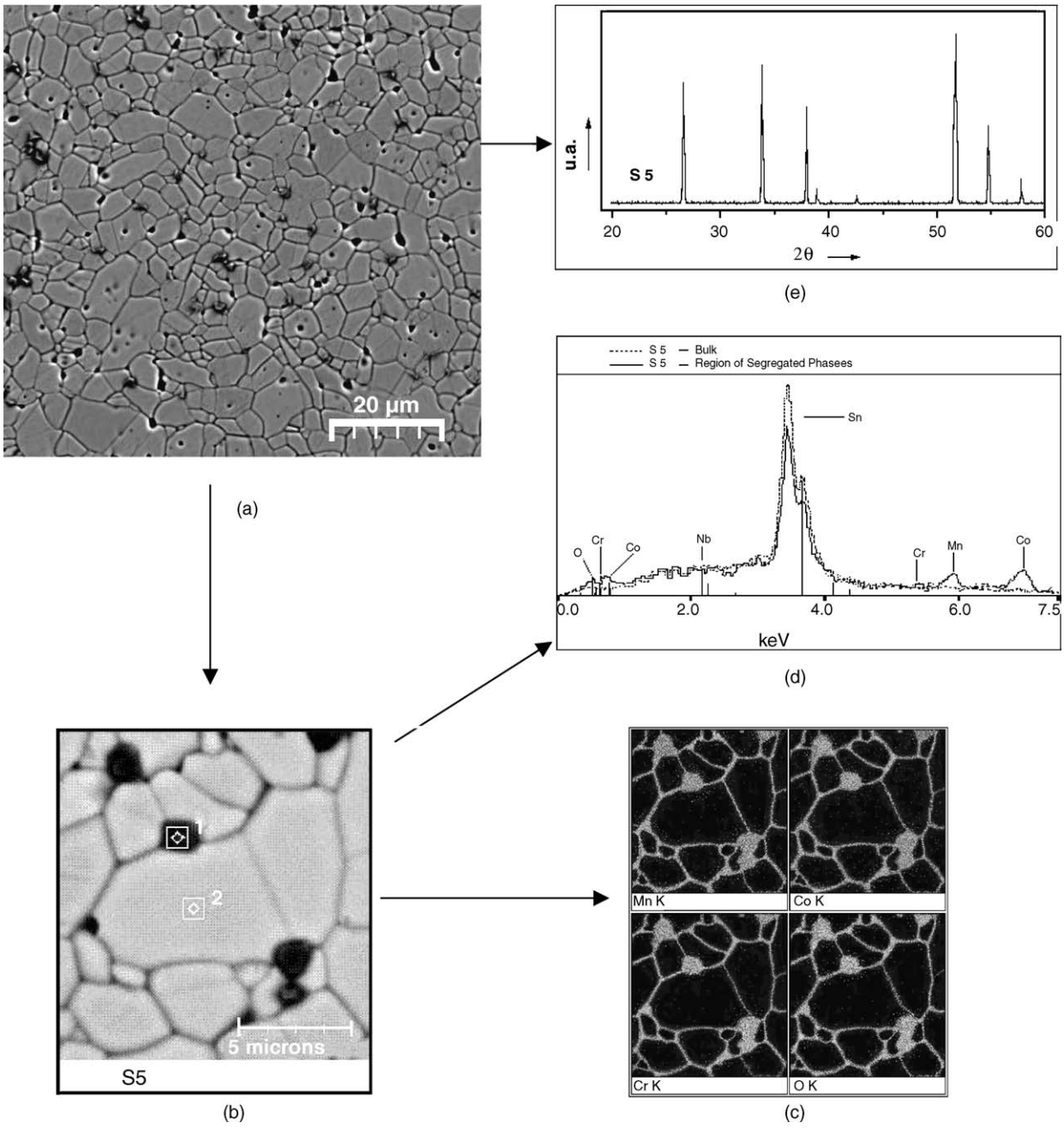

Fig. 2. (a, b) The micrographs (SEM) of the S5 composition sintered at 1300 °C for 1.5 h at two different magnification (1000×) and (5000×), respectively. (c, d) The energy dispersive spectroscopic (EDS) analysis accomplished by mapping of the material surface. (e) X-ray pattern of S5 composition.

pores and a lower relative density of the compositions with the increased MnO concentration. Increases in the MnO concentration are also accompanied by an increased amount of precipitate phase at triple points of the grain boundaries.

The micrographs of Figs. 1 and 2 show the heterogeneity found in the $SnO_2(Co_xMn_{1-x})O$-based ceramics when x decreased. In the samples containing larger MnO molar concentrations (or lower values of x), the precipitation at the grain boundaries increased, and this was also accompanied by an increase in intra- and inter-granular pores. Such an increase in porosity and precipitates interferes in the material's nonohmic electrical features, as discussed earlier herein. Fig. 1 illustrates the microstructures obtained for the S2 and S8 compositions, while Fig. 2 illustrates the microstructure obtained for the S5 composition. As can be seen in the S2 system (whose composition is devoid of chromium), the amount of manganese and/or cobalt precipitated at triple points is not substantial. On the other hand, the S8 composition, which contains Cr_2O_3 as dopant and a higher concentration of MnO, shows clear evidence of the presence of a large amount of precipitated phase, indicating that high concentrations of Cr_2O_3 decrease the solubility of MnO at the

Table 3
Values of leakage ($I_{leakage}$) current and the electric field corresponding to a current density of 0.05 mA cm^{-2} ($E_{0.05}$) as a function of molar concentrations of MnO and CoO in $SnO_2(Co_x, Mn_{1-x})O{\cdot}Nb_2O_5$-based varistor systems and $SnO_2(Co_x, Mn_{1-x})O{\cdot}Nb_2O_5$-based varistor doped with Cr_2O_3

System	$I_{leakage}$ (mA)	$E_{0.05}$ (V)
S1	0.03911	1170
S2	0.03943	1361
S3	0.04094	1689
S4	0.03855	3420
S5	0.04138	2468
S6	0.04407	3769
S7	0.04904	5725
S8	–	–

grain boundaries. This precipitate phase is found mainly in the triple junctions of the grain boundary region, similarly to what was reported in ref.[36]. Oliveira et al.[36] studied the microstructure of $SnO_2{\cdot}CoO$-based varistor systems doped with La_2O_3 and Pr_2O_3, using HRTEM equipped with EDS, and found that the precipitate phases were composed mainly of Co_2SnO_4 and $Pr_2Sn_2O_7$ at the grain boundary. These phases were also found mainly at the triple points of the grain boundary region.

Fig. 2a shows a SEM micrograph of the S5 composition, revealing the presence of a precipitated phase at the grain boundary. Fig. 2b shows a detailed region of the grain boundary of the S5 composition. Fig. 2c and d show an EDS analysis of bulk and precipitate phase at the grain boundary of the same region indicated in Fig. 2b. As can be seen in Fig. 2c and d, the precipitate phase in the grain boundary region is rich in Co, Mn, Cr and oxygen, while the grains are predominantly composed of SnO_2 and Nb. These results are congruent with the mechanism proposed for the formation of the potential barrier, corroborating results reported in the literature.[24,26,31]

3.2. Segregated and/or precipitated chromium dopant and the nonohimic features

As discussed in the previous section, Fig. 2 reveals the presence of manganese, cobalt and chromium in the grain boundary region. Manganese and cobalt influence not only the densification but also the electronic conduction of these materials, because they act as electronic acceptors in the forbidden region between conduction and the valence band. As mentioned earlier, the presence of such elements in the grain boundary region facilitates oxygen species enrichment at the grain boundary. Because these species are partially responsible for the formation of potential barriers, they contribute to increase the systems' nonlinearity coefficient. The features of the S4 composition, which showed a high α value and nonohmic features, can be explained by the combination of two major effects. Firstly, in this polycrystalline composition, the percolation paths parallel to the current through the non-active potential barrier are absent, likely due to the fact that there are sufficient segregated dopant metals (Mn and/or Co atoms) at the SnO_2–SnO_2 junction without a precipitate phase at the triple point, which occurs easily due to the absence of MnO (see also refs.[29,30]). Therefore, according to ref.,[31] parallel conduction through non-active barriers cannot contribute to decrease the α values because these parallel paths are eliminated by sufficient amounts of dopant homogeneously distributed in the SnO_2–SnO_2 junction.

The above discussion is summarized in the analysis shown in Table 2. This table presents the results of the breakdown electrical field (E_r), nonlinearity coefficient (α) and barrier per grain (ν_b), the latter obtained from the relation $\nu_b = E_r d$, in which d is the mean grain size. Table 2 also shows that all the results indicate the reversibility of α values upon reheating in an oxygen-rich atmosphere (re-O_2), which was conducted at 900 °C, as reported in the experimental section above. Furthermore, the greater the compositions' MnO and Cr_2O_3 concentrations, the higher the breakdown voltage in the presence of a higher leakage current of up to $x = 0.25$. This finding reinforces the conclusions of our analysis. Moreover, the S8 composition was highly resistant to electrical conduction, making it impossible to obtain an α

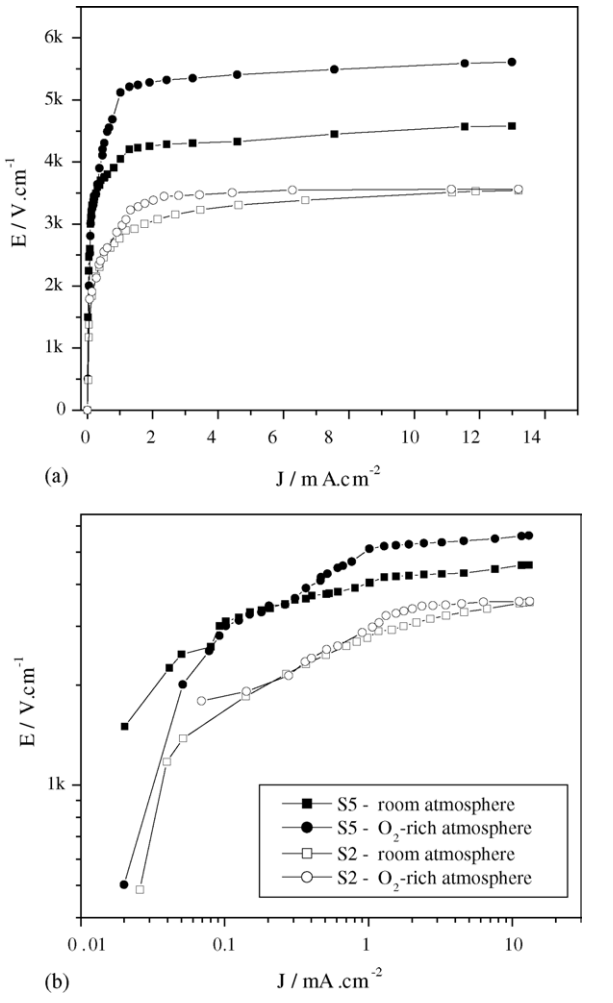

Fig. 3. *I–V* characteristic plot for S5 and S2 compositions thermally treated at 900 °C in room and oxygen-rich atmospheres. (a) Linear and (b) logarithmic plots.

value for this composition. The same held true for the S7 composition after it was subjected to a heat treatment in an oxygen-rich atmosphere. This behavior can be explained by the fact that, in the S8 composition, the combined addition of Cr_2O_3 and the large amount of MnO caused the elimination of the non-active SnO_2–SnO_2 junction responsible for parallel conduction and leakage current (Table 3), because the large amount of porosity at the triple point prevented phase precipitation at this point of the microstructure. This effect, combined with an abnormal increase of breakdown voltage, was responsible for the system's higher electrical resistance. Table 3 shows the leakage current obtained in the various compositions.

According to the model proposed in refs.[24,26] as previously discussed, the nonohmic properties of varistor systems are related with trapping states in the grain boundary region, and these states are likely related with the presence of oxygen species at the grain boundary interfaces. The concentration of oxygen species is controlled by defects, such as Cr'_{Sn}, Cr''_{Sn}, Co''_{Sn}, Mn''_{Sn}, V''''_{Sn}, which promote oxygen enrichment at the grain boundary. Therefore, the effect of oxygen enrichment on the nonohmic properties can be evidenced by heat-treating the samples in different atmospheres, oxygen-rich and/or poor. The effect of oxygen on the nonohmic properties is illustrated in Fig. 3 by plots of *J*–*E* for the S2 and S5 samples sintered at 1300 °C in static air and subsequently subjected to heat treatment in an oxygen-rich atmosphere. Table 4 summarizes the results obtained for the S2 and S5 compositions and others, showing the effect of the chromium dopant through a comparison with the systems that do not contain chromium oxide dopant. The results indicate that grain boundary oxygen enrichment efficiency is greater in the presence of chromium than in the presence solely of manganese and cobalt. This improvement in the systems' nonohmic properties in the presence of chromium is likely attributable to the affinity of Cr atoms for oxygen species, combined with their homogeneous presence in high concentrations in the microstructure's grain boundary region.

During the sintering process or heat treatment at 900 °C, oxygen may diffuse through the grain boundary region and this oxygen species reacts with segregated transition metals or with precipitate. The solid-state reactions of Eqs. (6)–(10) illustrate the influence of chromium on the oxygen enrichment of the grain boundary. This type of solid-state reaction causes the grain boundaries to rise to surface states, resulting in an increase of the mean height of the potential barrier, which usually leads to an increase of nonohmic properties.[24,26]

$$Cr''_{sn} + O_2 \Leftrightarrow Cr'_{sn} \cdot O'_{2(ads)}, \quad (6)$$

$$Cr''_{sn} + Cr'_{sn} \cdot O'_{2(ads)} \Leftrightarrow 2Cr'_{sn} \cdot O'_{(struct)}. \quad (7)$$

Cr^{2+} and Cr^{3+} are stable at high temperatures during heat treatment, and oxidation of the grain boundary may cause an increased presence of Cr^{2+} ($Cr_3O_4 \rightarrow Cr_2O_3 + CrO$) states, facilitating the oxygen enrichment of segregated particles and/or precipitates, according to Eqs. (6) and (7) and to the possible mechanisms illustrated below:

$$Cr''_{sn} + Cr'_{sn} \cdot O_{2(ads)} \Leftrightarrow Cr'_{sn} + Cr''_{sn} \cdot O_{2(ads)} \Leftrightarrow Cr'_{sn} + Cr'_{sn} \cdot O'_{2(ads)}, \quad (8)$$

$$Cr''_{sn} + Cr'_{sn} \cdot O'_{2(ads)} \Leftrightarrow 2Cr''_{sn} \cdot O_{str} \Leftrightarrow 2Cr'_{sn} \cdot O'_{str} \quad (9)$$

Table 4
Relative efficiency of Cr_2O_3 and MnO molar concentrations in the nonohmic features of the studied compositions after thermal treatment at 900 °C for 1 h in an O_2 flux of 2 L min^{-1}

Systems	Compositions	Ambient atmosphere	O_2 atmosphere	Variation (%)
S1	0.000% MnO_2 1.000% CoO 0.000% Cr_2O_3	$E_r = 4920$ $\alpha = 21$	$E_r = 5206$ $\alpha = 24$	6 14
S2	0.250% MnO_2 0.750% CoO 0.000% Cr_2O_3	$E_r = 2888$ $\alpha = 11$	$E_r = 3083$ $\alpha = 13$	7 18
S3	0.500% MnO_2 0.500% CoO 0.000% Cr_2O_3	$E_r = 3612$ $\alpha = 13$	$E_r = 3710$ $\alpha = 14$	3 12
S4	0.000% MnO_2 1.000% CoO 0.025% Cr_2O_3	$E_r = 4106$ $\alpha = 49$	$E_r = 4575$ $\alpha = 75$	11 53
S5	0.250% MnO_2 0.750% CoO 0.025% Cr_2O_3	$E_r = 4000$ $\alpha = 21$	$E_r = 5925$ $\alpha = 35$	48 66
S6	0.500% MnO_2 0.500% CoO 0.025% Cr_2O_3	$E_r = 5904$ $\alpha = 14$	$E_r = 6947$ $\alpha = 27$	17 92

$$Cr''_{sn} + Cr'_{sn} \cdot O'_{str} \Leftrightarrow Cr'_{sn} + Cr''_{sn} \cdot O'_{str} \Leftrightarrow Cr'_{sn} + Cr'_{sn} \cdot O''_{str}, \quad (10)$$

where $Cr'_{sn} = Cr^{3+}$; $Cr''_{sn} = Cr^{2+}$.

The theoretical studies conducted by Rantala[37–39] indicate that the band gap of SnO_2 bulk is about 3.6 eV and that the maximum of the valence band is created from 2p levels of oxygen atoms, while the minimum of the conduction band is created from 5s levels of tin atoms. The study foresaw the presence of surface states (levels) in the band gap, with many of these states relating to the missing bridge oxygen atoms (V_O^x). Chromium impurities in SnO_2 strongly affect the electrical properties of both bulk and surface. The authors' studies indicate that this is a consequence of the Cr 3d levels that emerge in the band gap. Bulk impurities produce deep levels near the valence band, while surface impurities create levels in the middle portion of the gap. These two levels act as an electron trap, favoring the adsorption of oxygen. In their study of Cr-doped varistor sensors, Sharma et al.[14,37] found that, when an oxygen molecule surfaces, it interacts with Cr metal atoms since there is an excess of electrons on the Cr metal ions. Thus, oxygen can easily be chemisorbed at Cr sites, bonding with Cr^{3+}. At ambient temperature, Cr metal ions also act as catalysts because surface Cr atoms easily get oxidized and can take 4+ effective valence, a mechanism that is illustrated by the reaction: $2Cr^{3+} + O_2 \rightarrow 2Cr^{4+}{-}O^-$, according to ref.[14] This appears to contradict Eqs. (6)–(10), since it means that $Cr'_{sn} \rightarrow Cr^x_{Sn} + e \rightarrow O_2^-$. However, it is important to point out that our reactions are expected to occur at higher temperatures; hence, electrons from other states of the forbidden band or conduction band can stabilize Cr^{3+} and Cr^{2+} valences. At ambient temperature, the CrO_x unit may be considered the primary building block for the nucleation of chromium oxide clusters (Cr metals from the bulk to the grain boundary, in the present case). All these results are consistent with the reversibility of the α values in the varistor systems, inasmuch as the temperature and oxygen-rich atmosphere can convert CrO_2 to $Cr_{2-y}O_3$ and/or to $Cr_{3-y}O_4$, which have higher acceptor features than the bulk. Therefore, during heat treatment in N_2-rich atmospheres, the acceptor features of $Cr_{2-y}O_3$ and/or $Cr_{3-y}O_4$ may be reduced by a decrease in the y values. Hence, it can be stated that Cr sites serve to capture oxygen from the environment, but the formation of acceptor features at grain boundaries are attributable to $Cr_{2-y}O_3$ and/or $Cr_{3-y}O_4$ states. Accordingly, the mechanism is highly reversible due to a reversibility of a higher "acceptor character" favored in O_2-rich atmospheres or a lower "acceptor character" favored in N_2-rich atmospheres.

York et al.[40] stated that Cr_2O_3 displays irreversible oxygen dissociation at ambient temperature, corresponding mainly to Cr=O, and reversible molecular oxygen absorption, suggested as $O_2{}^-$. It should be pointed out that, in the scheme of Eqs. (9) and (10), Cr'_{sn} and Cr''_{sn} illustrate the favoring of oxygen adsorption with dissociation at the heat treatment temperature, with good reversibility evidenced by the reversibility of α values and the breakdown voltage listed in Table 4, as reported in previous papers[22–24,26–28].

In their theoretical calculation of chromium oxide clusters, Veliah et al.[41] found that CrO_n-type clusters are more stable than Cr_mO_n-type clusters. The CrO_n-type clusters presented Cr–O bonds with covalent and polar features. They also found a higher gap in CrO_n-type clusters. In the Cr–O-type bond, they observed an electronic density transfer from the molecular orbital of "Cr" to "O" atom (from $3d_{Cr}$ and $4s_{Cr}$ to $2p_O$). In the Cr_mO_n-type clusters, the charge transfer occurred mainly between Cr–Cr bonds.

The above discussion, which was based on a theoretical analysis of chromium clusters, reinforces the mechanisms discussed herein according to the affinity of Cr atoms for oxygen, in agreement with the potential barrier formation mechanism described in previous papers[23,24,26].

4. Conclusions

The results discussed in this paper allowed for a correlation to be made between the MnO concentration and the amount of precipitated phase at triple points of the grain boundary region. Correlations were also found between the MnO concentration and the samples' relative density. MnO proved to be deleterious to nonohmic properties, inasmuch as it gave rise to a heterogeneous microstructure that contributed to the formation of a non-active potential barrier in SnO_2–SnO_2-type junctions, creating a path for the current. As a result, the presence of MnO has the effect of increasing the system's leakage current.

With regard to the Cr_2O_3 effect, Cr_2O_3 was found to facilitate the homogeneous enrichment of grain boundaries with oxygen species, increasing the performance of the nonohmic features of SnO_2-based varistor systems.

Acknowledgements

The authors gratefully acknowledge the support of the following Brazilian research financing agencies: FAPESP/CEPID, CNPq/PRONEX and CAPES.

References

1. Castro, M. S. and Aldao, C. M., *Appl. Phys. Lett.*, 1992, **63**, 1077.
2. Gupta, T., *J. Am. Ceram. Soc.*, 1990, **73**, 1817–1840.
3. Leite, E. R., Varela, J. A. and Longo, E., *J. Appl. Phys.*, 1992, **72**, 147.
4. Bueno, P. R., Camargo, E., Longo, E., Leite, E. R., Pianaro, S. A. and Varela, J. A., *J. Mater. Sci. Lett.*, 1996, **15**, 2048.
5. Bueno, P. R., Cassia-Santos, M. R., Simões, L. G. P., Gomes, J. W. and Longo, E., *J. Am. Ceram. Soc.*, 2002, **85**, 282–284.
6. Pianaro, S. A., Bueno, P. R., Longo, E. and Varela, J. A., *J. Mater. Sci. Lett.*, 1995, **14**, 692–694.
7. Pianaro, S. A., Bueno, P. R., Olivi, P. and Longo, E., *J. Mater. Sci. Lett.*, 1997, **16**, 634–637.

8. Pianaro, S. A., Bueno, P. R., Olivi, P., Longo, E. and Varela, J. A., *J. Mater. Sci.: Mater. Electron.*, 1998, **9**, 158–165.
9. Pianaro, S. A., Bueno, P. R., Longo, E. and Varela, J. A., *Ceram. Int.*, 1999, **25**, 1–6.
10. Jarzebski, Z. M. and Marton, J. P., *J. Electrochem. Soc.*, 1976, **123**, 299C–310C.
11. Jarzebski, Z. M. and Marton, J. P., *J. Electrochem. Soc.*, 1976, **123**, 199C–205C.
12. Cox, D. F., Fryberger, T. B. and Semancik, S., *Phys. Rev. B*, 1988, **38**, 2072–2083.
13. Moulson, A. J. and Herbert, J. M., *Electroceramics Materials, Properties and Application*. Chapman & Hall, London, 1993.
14. Sharma, R. K., Bhatnagar, M. C. and Sharma, G. L., *Sens. Actuators B*, 1997, **45**, 209.
15. Fagan, F. G. and Amararakoon, V. R. W., *J. Am. Ceram. Soc.*, 1993, **72**, 119–130.
16. Castro, M. S. and Aldao, C. M., *J. Eur. Ceram. Soc.*, 1998, **18**, 2233–2239.
17. Bacelar, W. K., Oliveira, M. M., Souza, V. C., Longo, E. and Varela, J. A., *J. Mater. Sci.: Mater. Electron.*, 2003, **13**, 409.
18. Cerri, J. A., Leite, E. R., Gouvea, D. and Longo, E., *J. Am. Ceram. Soc.*, 1996, **79**, 799–804.
19. Varela, J. A., Cerri, J. A., Leite, E. R., Longo, E., Shamsuzzoha, M. and Bradt, R. C., *Ceram. Int.*, 1999, **25**, 253–256.
20. Yongjun, W., Jinfeng, W., Hongcun, C., Weilie, Z., Peilin, Z., Huomin, D. and Lianyi, Z., *J. Phys. D: Appl. Phys.*, 2000, **33**, 96–99.
21. Yongjun, W., Jinfeng, W., Hongcun, C., Weilie, Z., Peilin, Z., Huomin, D. and Lianyi, Z., *Eur. Phys. J.: Appl. Phys.*, 2000, **11**, 155–158.
22. Bueno, P. R., Pianaro, S. A., Pereira, E. C., Bulhões, L. O. S., Longo, E. and Varela, J. A., *J. Appl. Phys.*, 1998, **87**, 3700–3705.
23. Bueno, P. R., Cassia-Santos, M. R., Leite, E. R., Longo, E., Bisquert, J., Garcia-Belmonte, G. and Fabregat-Santiago, F., *J. Appl. Phys.*, 2000, **88**, 6545–6548.
24. Bueno, P. R., Leite, E. R., Oliveira, M. M. and Orlandi, M. O., *Appl. Phys. Lett.*, 2001, **79**, 48–50.
25. Bueno, P. R., Oliveira, M. M., Bacelar-Junior, W. K., Leite, E. R., Longo, E., Garcia-Belmonte, G. and Bisquert, J., *J. Appl. Phys.*, 2002, **91**, 6007–6014.
26. Bueno, P. R., Oliveira, M. M., Bacelar-Junior, W. K., Leite, E. R. and Longo, E., *J. Appl. Phys.*, 2002, **91**, 6007–6014.
27. Leite, E. R., Nascimento, A. M., Bueno, P. R., Longo, E. and Varela, J. A., *J. Mater. Sci.: Mater. Electron.*, 1999, **10**, 321–327.
28. Cassia-Santos, M. R., Bueno, P. R., Longo, E. and Varela, J. A., *J. Eur. Ceram. Soc.*, 2000, **21**, 161–167.
29. Bueno, P. R., Orlandi, M. O., Simões, L. G. P., Leite, E. R., Cerri, J. A. and Longo, E., *J. Appl. Phys.*, 2004, **96**, 2693–2700.
30. Orlandi, M. O., Bueno, P. R., Bomio, M. R. D. and Longo, E., *J. Appl. Phys.*, 2004, **96**, 3811–3917.
31. Simões, L. G. P., Bueno, P. R., Oliveira, M. M., Leite, E. R. and Longo, E., *J. Electroceram.*, 2003, **10**, 63–68.
32. Turton, C. N. and Turton, T. I., *The Oxide Handbook*. IFI/Plenum, New York, 1973, pp. 378–379.
33. Paria, M. K., Basu, S. and Paul, A., *Trans. Indian Ceram. Soc.*, 1983, **42**, 90.
34. Han, J. H. and Kim, D. Y., *J. Am. Ceram. Soc.*, 1998, **18**, 75.
35. Kim, J. J., Kim, B. K., Song, B. M. and Kim, D. Y., *J. Am. Ceram. Soc.*, 1987, **70**, 734.
36. Oliveira, M. M., Soares Jr., P. C., Bueno, P. R., Leite, E. R., Longo, E. and Varela, J. A., *J. Eur. Ceram. Soc.*, 2003, **23**, 1875–1880.
37. Lantto, V. and Golovanov, V., *Sens. Actuators B*, 1995, **24–25**, 614.
38. Rantala, T. S. and Lantto, V., *Surf. Sci.*, 1996, **352–354**, 765–770.
39. Rantala, T. S., Lantto, V. and Rantala, T., *Sens. Actuators B*, 1998, **47**, 59–64.
40. York, S. C., Abee, M. W. and Cox, D. F., *Surf. Sci.*, 1999, **437**, 386.
41. Veliah, S., Xiang, K.-H., Pandey, R., Recio, J. M. and Newsan, J. M., *J. Phys. Chem. B*, 1998, **102**, 1126.